ALMA Memo No. 497

ANALYSIS OF WIND DATA GATHERED AT CHAJNANTOR

Juan Pablo Pérez Beaupuits [1], Angel Otárola [1], Fredrik T. Rantakyrö [1], Roberto C. Rivera [1], Simon J. E. Radford [2], Lars-Åke Nyman [1]

[1] European Southern Observatory, Casilla 19001 - Santiago de Chile

[2] National Radio Astronomy Observatory, 949 North Cherry Avenue, 5th Floor, Tucson, AZ 85721

2004 May 7

Abstract

A general description and statistics of the wind speeds and directions registered at the ALMA site during 2001 and 2002 are presented. Measurements from different wind directions within 22.5º (in azimuth), topographic sectors and two markedly different daily periods were obtained. Spectra of the wind turbulence are presented for three wind speed conditions. During the diurnal period the convective turbulence and mean wind speed determine the shape and magnitude of the wind spectra, whereas in the nocturnal period the effects of the mechanical turbulence, such as the wind shear and surface roughness together with the mean wind speed, become relevant. No significant differences were found between the spectra obtained from three topographic sectors in the diurnal period, whereas in the nocturnal period a statistical test showed a significant difference for a particular topographic sector and for a given wind speed range, reflecting changes in the wind spectrum structure due to the local topography. General models of average spectra were found for three mean wind speeds, in the diurnal and nocturnal periods. Relations between the models and the mean wind speed were found. These relations makes it possible to estimate the spectral behaviour of the wind at the ALMA site for different mean wind speeds, which will be useful in the study of the wind loading on the antenna structure and pointing. Based on the results we can also conclude that the performance of the ALMA antenna regarding wind load is expected to be better for both day time and nigh time periods.

Key Words: **WIND SPECTRUM – WIND TURBULENCE – COMPARISON TEST – SITE TESTING**

1. Introduction

Large radio telescopes operated at short wavelengths have small beam sizes and their pointing accuracy requirements thus become more demanding. The largest sources of errors are usually gravitational and thermal deformations, which are varying slowly with time. Extremely high accuracy pointing requirements present additional problems due to the potential dynamic response to the wind loading on the antenna structure (Smith et al., 2000).

The wind loading effect is caused by mechanical turbulence resulting from the air stirred by objects on the ground such as buildings, trees, hills, etc, and from the convective turbulence produced by instabilities in the atmosphere caused by solar heating. Mechanical turbulence also results from friction due to the interaction between the air (shear stress) and the ground itself (roughness).

One of the most important features of the wind turbulence is its spectrum. The basic form of the spectrum of the longitudinal wind turbulence during horizontally homogenous and neutrally stratified atmospheric conditions is shown in Figure 1.1. The larger eddies at the low frequency end of the spectrum (production range) are constantly being generated by the relative motion between the free-stream gradient flow and the stationary air near the ground, which feeds energy to the turbulence. At the other end of the spectrum (dissipation range), viscous shear stresses become significant when eddies have been reduced to a sufficiently small size (approximately 1 cm), allowing the turbulent energy to be dissipated. Between these two extremes, the energy is continuously transferred from larger to smaller eddies as the larger eddies are progressively broken down; this region over which the energy cascades from larger to smaller eddies with no significant energy input or dissipation is known as the *inertial subrange*.

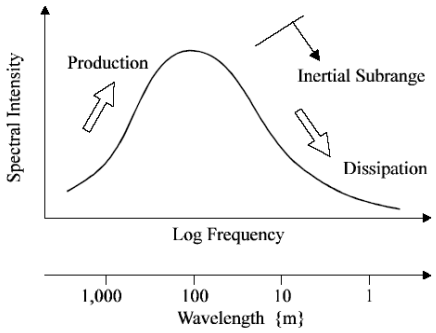

Figure 1.1 Schematic of wind turbulence spectrum

The inertial subrange has been extensively studied under near neutral atmospheric condition and several models have been found for different kind of terrain (Davenport, 1961; Kaimal et al., 1972 and 1976; Antoniou et al., 1992). The lower frequency range (between frequency 0 Hz and the lower end of the inertial subrange) varies with the local atmospheric and topographic conditions, so the spectrum cannot be described by a universal relation (Simiu and Scalan, 1996).

In this work the wind spectrum have been computed for different wind speed conditions. We have applied a variation of the methodology used by Antoniou et al. (1992), Antebi et al. (1997) and Hiriart et al. (2001), in order to study how the wind spectra are affected by the local atmospheric and topographic conditions at the site.

The present work is organized as follows: in §2 we describe the site**,** in §3 the instruments and wind statistics are described**,** in §4 the wind data is classified**,** in §5 wind spectra are determined**,** in §6 the wind spectra are discussed**,** in §7 models of the wind spectra for different mean wind speeds are presented and a comparison with a reference model for the specifications of the ALMA antennas is discussed, in §8 the main conclusions of this work are presented**,** and finally in §9 further work is suggested and discussed.

2. Description of the Site

The site of study is situated in the Chajnantor area, 60 km North-East of San Pedro de Atacama, in the 2nd Region of Chile. The area in which the measurements were done is about 5000 m above sea level. The geomorphology of the site is nearly flat, surrounded by hills, mountains and depressions. The terrain is about 25000 hectares of land and is formed mainly of sand and rocks, without significant ground cover. During part of the local winter season the area is almost completely covered with snow. Figure 2.1 shows a digital elevation model of Chajnantor zone of about 25 km^2 including the area where several meteorological instrument are installed. The place where the instruments are located is indicated by an arrow.

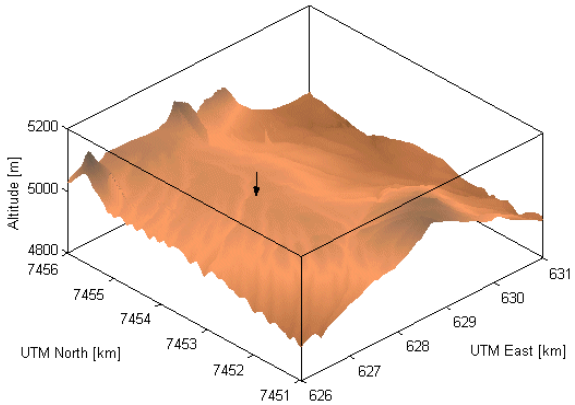

Figure 2.1 Digital elevation model of Chajnantor area. Horizontal axes are in km for the UTM Zone 19 Northing-Easting coordinates.

3. Instrumentation and Wind Statistics

3.1 Wind Speed Measurements

A RISØ P2546 cup-anemometer was used to collect wind speed data registered at 1 Hz sampling rate. It is installed at a height of 7.8m (a 5.2m high steel mast, on the top of a 2.6m high container). The measured wind speed of the cup-anemometer is an averaged one-dimensional quantity. The input to the cup-anemometer is a time dependent 3D wind speed vector $\vec{U} = (u, v, w)$ with a longitudinal component *u*, a transversal component *v*, and a vertical component *w*. The RISØ P2546 cup-anemometer has a cosine angular response, which causes the vertical component *w* to be automatically filtered out, and the definition of measured wind speed of the cup-anemometer is the "horizontal" wind speed. The longitudinal and transversal wind speed components yields a 2D averaged measurement (Pedersen 2003):

$$\mu \equiv |\vec{U}| = \int_t \sqrt{u^2 + v^2} \ . \tag{1}$$

The cup-anemometer data covers, with some gaps, from April 2001 to December 2002. The amount of available data represents about 36.5% of 2001 and about 60.8% of 2002. The available proportion of data for each month during both years is summarized in Table 3.1. The missing data was caused by power supply problems and communications problems to the instrument. In order to reduce the effect of missing data, we have merged the data from both years to obtain enough representative data for each month. For this synthesized year the proportion of available data amounts to 75.8% of the ideal (12 months) data.

The histogram of this synthesized year is shown in Figure 3.1a. The bins have a width of 1 [m/s] and the quartiles Q_1(25%), Q_2(50%) and Q_3(75%) are 4.74 m/s, 7.69 m/s and 10.93 m/s, respectively. Of special interest for the antenna operation is the proportion of registered wind speed above 20 m/s, which is about 0.76% of the available data, i.e. less than 3 days a year.

3.2 Wind Direction Measurements

A propeller-anemometer installed by NRAO at about 7 m over the ground at Chajnantor was used to collect wind direction data. Due to power supply problems and noise in some of the measurements, only about 43.9% of the ideal total data is available for 2001, and 25.4% for 2002. In the same way, as we have done for the cup-anemometer data, we synthesized a year containing all data from the propeller-anemometer. This data covers about 50.6% of the total possible data to be gathered in one year at a 10 minute sampling. The proportion of available data for each month is summarized in Table 3.1.

Figure 3.1b shows wind direction histograms (windrose) for the synthesized year. The windrose consists of 16 bins, 22.5º in width. This figure shows the central angle of each bin and the proportion (in percentage) of wind direction data respect to a full year. This windrose plot shows the wind blows predominantly from West to East. An important exception to this predominant condition occurs mainly during the months from January to March, corresponding to the Bolivian winter (Radford 2004, Bustos et al. 2000), when the wind blows from East to West.

Detailed statistics for wind speeds and directions, taking into account all data gathered from 1995 through 2003, can be found in Radford (2004) and shows a median wind speed of about 6m/s. Meanwhile, in this work the median value for the synthesized year reaches about 8m/s. This difference is explained by the fact the data in this work is intrinsically biased towards high values because the major proportion of the data comes from those months of higher wind speeds. A comparison between the wind speed data registered by the different meteorological instruments installed at Chajnantor can be found in the appendix of this work.

TABLE 3.1 AVAILABLE PROPORTION OF DATA FOR EACH MONTH OF YEARS 2001 AND 2002, REGISTERED WITH THE CUP AND PROPELLER ANEMOMETERS.

	CUP-ANEMOMETER			PROPELLER-ANEMOMETER		
Month	***Available Data in 2001 [%]***	***Available Data in 2002 [%]***	***Total Available Data 2001 & 2002 [%]***	***Available Data in 2001 [%]***	***Available Data in 2002 [%]***	***Total Available Data 2001 & 2002 [%]***
January	0.0	70.79	70.79	72.40	0.0	72.40
February	0.0	87.91	87.91	71.63	40.15	71.63
March	0.0	22.90	22.90	71.48	20.12	71.48
April	0.21	63.15	63.36	72.38	47.69	72.38
May	53.92	91.63	91.63	3.25	38.53	38.53
June	7.23	91.40	91.40	0.0	28.36	28.36
July	24.28	59.15	83.43	0.0	0.0	0.0
August	29.41	49.07	78.48	0.0	0.0	0.0
September	91.39	68.33	91.39	54.28	0.0	54.28
October	91.14	91.60	91.60	70.88	3.0	70.88
November	92.82	36.82	92.82	71.64	72.11	72.11
December	46.01	0.0	46.01	42.18	58.27	58.27
Total	***36.54***	***60.80***	***75.78***	***43.89***	***25.44***	***50.62***

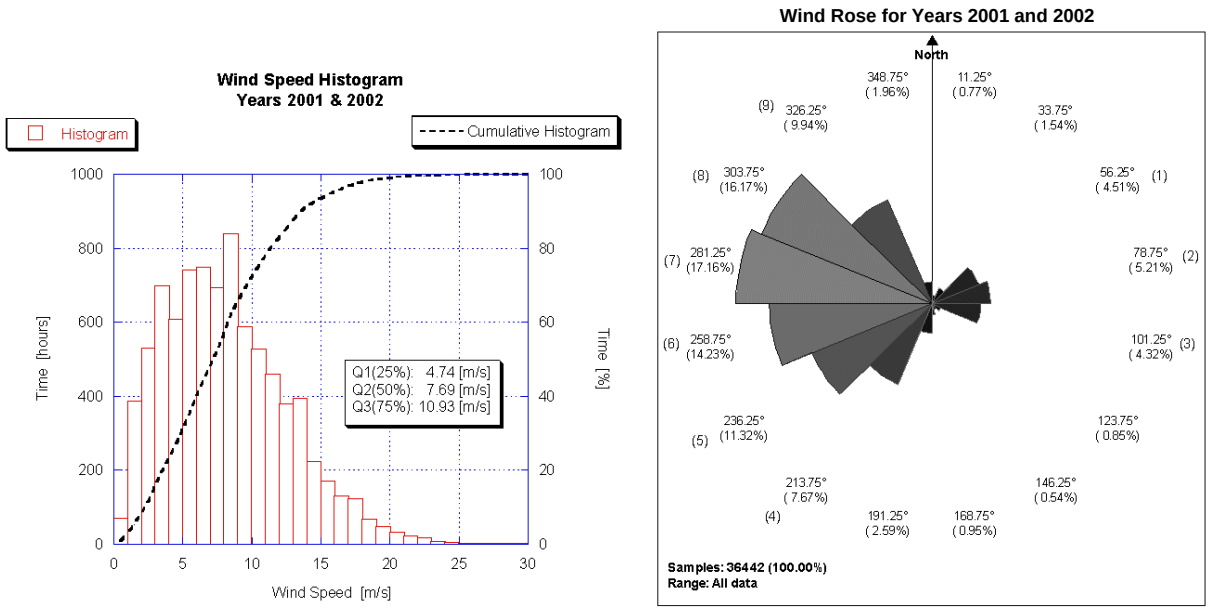

(a) (b)

Figure 3.1 (a) Wind speed histogram for data collected during 2001 and 2002. The width of the bins is 1 m/s. The quartiles Q_1, Q_2 and Q_3 of the wind speed are 4.74 m/s, 7.69 m/s and 10.93 m/s, respectively. (b) Windrose histogram for all data obtained during 2001 and 2002 with the propeller-anemometer at Chajnantor. Each bin has a width of 22.5°. The angle of each bin is shown, as well as the corresponding proportion (%) of wind speed data. The most relevant bins of data are numerated. The wind blows mainly from West to East.

4. Classification of Wind Data

4.1 Wind Speed Conditions

With the aim to cover and analyze the different magnitudes of wind speeds at Chajnantor, the following four wind speed conditions (ranges) were defined based on the quartiles described in section 3.1:

- *Weak* wind speed condition: wind speeds lower than L_1 [m/s],
- *Medium Weak* wind speed condition: wind speeds between L_1 and L_2 [m/s],
- *Medium Strong* wind speed condition: wind speeds between L_2 and L_3 [m/s],
- *Strong* wind speed condition: wind speeds equal or grater than L_3 [m/s],

where the limits L_1, L_2 and L_3 are defined as: $L_1=(Q_1+Q_2)/2=6.21$ m/s, $L_2=(Q_2+Q_3)/2=9.31$ m/s, and $L_3 = L2 + (L2 - L_1)=12.41$ m/s. These conditions and the proportion of data within each range are summarized in Table 4.2. The largest proportion of data is dominated by the *weak* wind speed condition. This wind range is of little interest in this work because the wind load generated by these wind speeds range has no significant effect on the antenna structure and pointing. Besides, it is well known that at low wind speeds cup-anemometers are affected by non-linear effects (Yahaya and Frangi 2003).

TABLE 4.2 WIND SPEED CONDITIONS AND CORRESPONDING PROPORTION OF DATA

Wind Speed Condition	Range of Wind Speed (WS) [m/s]	Proportion of Data [%]
Weak	$0 \leq WS < 6.21$	37.44
Medium Weak	$6.21 \leq WS < 9.31$	27.07
Medium Strong	$9.31 \leq WS < 12.41$	18.17
Strong	$WS \geq 12.41$	17.32

4.2 Definition of Night and Daytime Periods

The wind speeds show a daily cycle due to the transfer of energy from solar radiation during day time, which makes the wind speed increase, and the consecutive cooling and loss of energy during the night time then reduces the wind speed. In order to identify the two periods in the daily wind speed cycle, we computed an average day of wind speeds by averaging all data collected during 2001 and 2002 respectively, in bins of 10 minutes (Figure 4.1a). The daily cycle is clearly seen for both years. Figure 4.1b shows the average daily cycle computed using all data from both years. There is a period of higher wind speeds during day time, roughly between 12 and 24h UT with a peak at about 20h UT. Night time period is very calm and stable and shows the lowest wind speeds.

In order to determine the wind spectra for each of these periods it is necessary to define their start and stop times. We used the *weak* wind speed condition (wind speeds below 6.21 m/s) as a threshold to distinguish between the two periods. From the data presented in Figure 4.1b we define the night time (nocturnal cycle) as the period of time between 1 and 11 UT, and the day time (diurnal cycle) for the remaining part of the day. The definition of the diurnal and nocturnal periods is based on an average day computed from the whole database, and seasonal effects are expected.

The histograms of wind speed for the diurnal and nocturnal periods are presented in Figure 4.2. The proportion, relative to the total amount of data, of wind speeds falling within each wind speed condition for diurnal and nocturnal periods is summarized in Table 4.3. The proportion of wind speeds registered above 20 m/s for the diurnal and nocturnal periods are 0.55% and 0.21% respectively. If data had been obtained 100% of the time, it is likely that these proportions would have increased. This is of interest for the case of stowing the antenna, due to high winds, for safety and operational reasons.

The windroses for the diurnal and nocturnal periods are shown in Figure 4.3. During the diurnal period the wind blows mainly from west to east, with a significant proportion of time when it blows from north-west and south-west. In contrast, the wind blows predominantly from the north-west direction during the nocturnal period. The proportion of time when the wind blows from east to west is similar during both periods.

The definition of the two periods has some implication on antenna operations regarding wind loads. The nocturnal period offers the best condition for astronomical observations, because of both: the low wind speeds and the better atmospheric transparency (see webpage http://www.tuc.nrao.edu/mma/sites/Chajnantor/data.c.html).

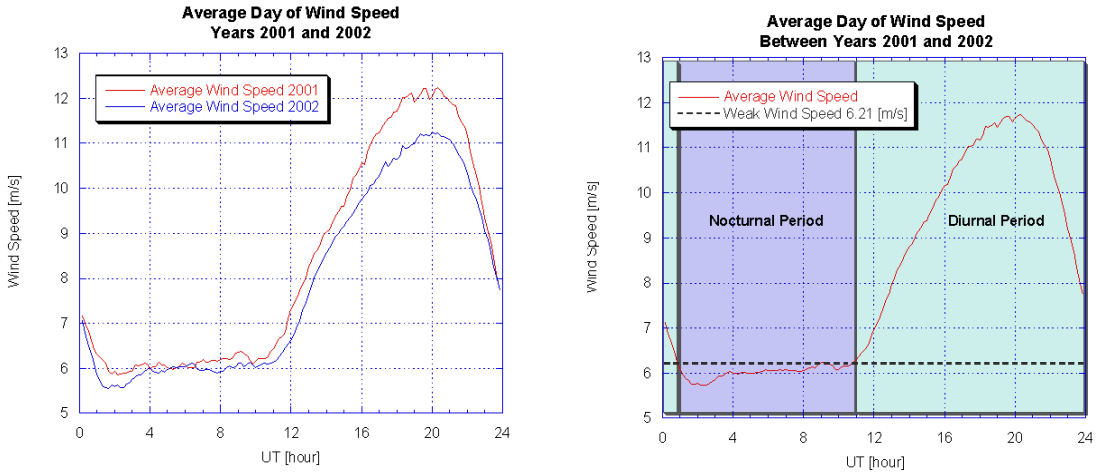

(a) (b)

Figure 4.1 (a) Average days of wind speed during years 2001 and 2002. The series are the mean of the average days for each available month of both years. The daily cycles of wind speed is clearly seen in the figure, and both average days are very similar during night time, but presents a small difference (about 1 m/s) during day time, specifically between 18 and 22 hrs. (b) This figure shows the mean between the average days of years 2001 and 2002. Taking the *weak* wind speed condition as threshold we can define the diurnal period from about 11 to 1 UT hour, and the nocturnal period from the remaining period of time (i.e., between 1 and 11 UT hour).

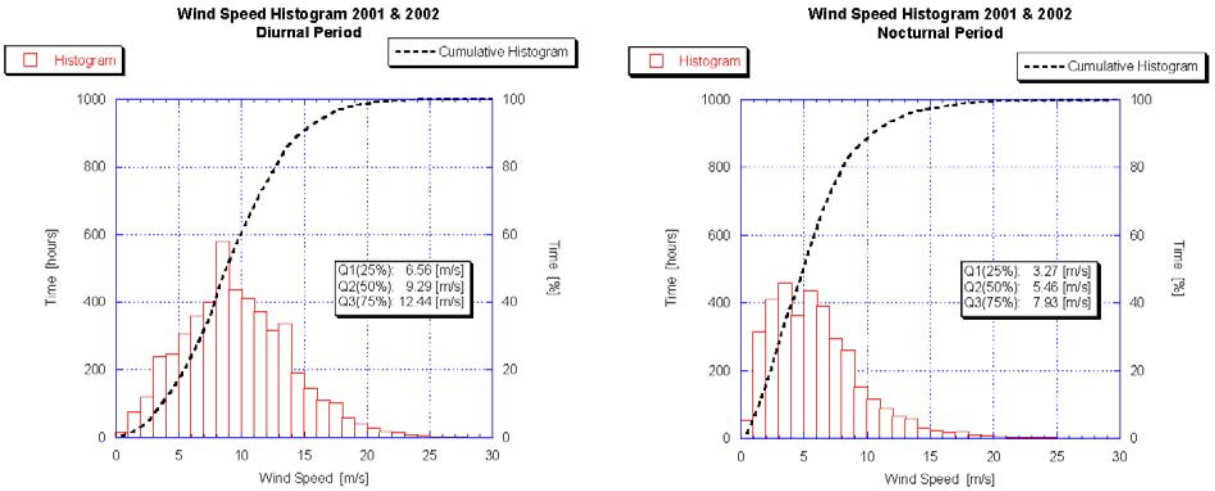

(a) (b)

Figure 4.2 (a) and (b) Wind speed histogram of the diurnal and nocturnal periods, respectively, for 2001 and 2002 together.

TABLE 4.3, PROPORTION RELATIVE TO THE TOTAL AVAILABLE DATA FOR THE DIURNAL AND NOCTURNAL PERIODS WITHIN EACH WIND SPEED CONDITION

Wind Speed Condition	Diurnal Period [%]	Nocturnal Period [%]
Weak	12.58	24.86
Medium Weak	16.39	10.68
Medium Strong	14.21	3.96
Strong	14.56	2.76

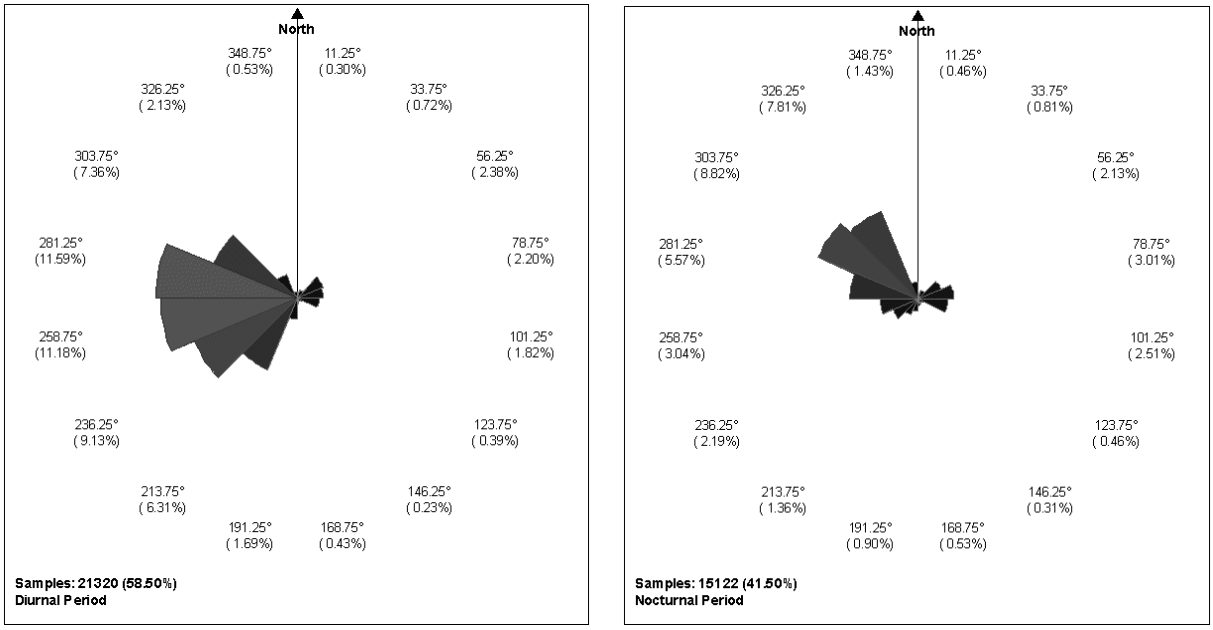

(a) (b)

Figure 4.3 Windrose histograms for diurnal (a) and nocturnal (b). The figure shows that the wind blows mainly from West to East in the diurnal period, with some periods of time blowing from north-west and south-west directions. During the nocturnal period the wind blows predominantly from north-west directions. The proportion of time when wind blows from east to west is similar in both periods.

5. Wind Spectra

5.1 Selection of Wind Data

The wind spectrum was determined using data taken at different wind speeds and wind directions. The cup anemometer does not give any information about the wind direction. Therefore, the wind direction data from the NRAO's propeller anemometer had to be used, with the sampling rate of 10 minutes. Thus, in order to assign a wind direction to the wind speed data, the minimum length in the wind speed data series was also set to 10 minutes. All available 10 minutes blocks from the cup-anemometer data were separated in diurnal and nocturnal periods, according to the selection criteria explained in section 4. Because the roughness length z_0 (the distance above ground level where the wind speed theoretically should be zero) depends on ground condition we decided to further divide the wind database for two ground conditions; with and without snow. In 2001 only about 9% of the year the site was covered by snow, and 13% of the year in 2002 (this information is summarized in Table 5.1). However, the wind speed data available for those days was considered too few to draw any reliable conclusions, so we decided not to include it in our analysis.

The turbulence of the wind may also depend on wind direction due to the influence of local topography (Antoniou et al. 1992, Barthelmie et al. 1993, Antebi et al. 1997). Considering the proportion of data shown in Figure 4.3 we decided to use data collected from wind directions in sectors of 22.5º wide, centred at 236.25º, 258.75º and 281.25º in azimuth (named *sectors 5, 6 and 7,* respectively in Figure 3.1) for the diurnal period, and 281.25º, 303.75º and 326.25º (*sectors 7, 8 and 9,* respectively) for the nocturnal period.

There are in total 9 cases for analysis in each period: three main directions for each of the three wind speed conditions (*Medium Weak*, *Medium Strong* and *Strong*). Tables 5.2 and 5.3 summarize the data for both periods. These tables show the number of blocks used in the analysis of each sector, the average wind speed, the average wind direction and average turbulence intensity (the ratio between the root mean square value of the wind series and its mean wind speed), together with

respective standard deviations. The average wind direction corresponds to the average of the wind directions associated from the propeller anemometer to each block of 10 minutes of wind speed data.

TABLE 5.1 NUMBER OF DAYS WITH CHAJNANTOR GROUND TOTALLY COVER WITH SNOW ARE INDICATED FOR EACH MONTH OF 2001 AND 2002. ALSO THE TOTAL PROPORTIONAL AMOUNT OF DAYS IS SHOWN.

Month	**Period with Snow in 2001 [days]**	**Period with Snow in 2002 [days]**	**Average Days with Snow 2001 & 2002 [%]**
February	0	5	8.93
March	9	3	19.35
April	3	0	5.00
May	9	16	40.32
June	0	13	21.67
July	0	9	14.52
August	4	0	6.45
September	5	0	8.33
October	2	3	8.06
Total days	***32***	***49***	***11.10***

TABLE 5.2, DATA WITHOUT SNOW COVERING THE GROUND USED IN THE ANALYSIS OF WIND SPEED MEASURED AT CHAJNANTOR FOR THE DIURNAL PERIOD.

Sector No.	Wind Condition	Number of Blocks used	Average Wind Speed [m/s]	Average Wind Direction [deg]	Average Turbulence Intensity [%]
5	*Medium Weak*	289	8.02 ± 0.85	237.97 ± 6.35	14.16 ± 5.58
6	*Medium Weak*	342	8.06 ± 0.76	258.77 ± 6.56	14.49 ± 5.41
7	*Medium Weak*	350	8.04 ± 0.84	280.86 ± 6.67	13.92 ± 5.25
5	*Medium Strong*	295	10.66 ± 0.74	237.48 ± 6.55	17.81 ± 4.56
6	*Medium Strong*	520	10.60 ± 0.71	259.62 ± 6.34	17.71 ± 5.09
7	*Medium Strong*	414	10.75 ± 0.74	280.98 ± 6.56	17.67 ± 4.99
5	*Strong*	70	14.44 ± 1.58	238.91 ± 6.39	24.17 ± 4.88
6	*Strong*	215	15.49 ± 1.98	261.03 ± 6.36	23.64 ± 4.37
7	*Strong*	365	15.88 ± 2.35	281.27 ± 6.81	23.36 ± 4.82

TABLE 5.3, DATA WITHOUT SNOW COVERING THE GROUND USED IN THE ANALYSIS OF WIND SPEED MEASURED AT CHAJNANTOR FOR THE NOCTURNAL PERIOD.

Sector No.	Wind Condition	Number of Blocks used	Average Wind Speed [m/s]	Average Wind Direction [deg]	Average Turbulence Intensity [%]
7	*Medium Weak*	195	7.71 ± 0.90	282.77 ± 6.55	6.49 ± 1.71
8	*Medium Weak*	519	7.72 ± 0.81	304.19 ± 6.25	7.34 ± 2.25
9	*Medium Weak*	308	7.40 ± 0.72	324.82 ± 5.55	7.46 ± 2.96
7	*Medium Strong*	153	10.26 ± 0.62	283.20 ± 6.09	9.08 ± 2.12
8	*Medium Strong*	134	10.34 ± 0.76	302.97 ± 6.83	10.89 ± 2.76
9	*Medium Strong*	50	10.51 ± 0.69	320.24 ± 3.58	12.45 ± 2.22
7	*Strong*	9	15.14 ± 1.68	283.08 ± 6.75	18.28 ± 3.16
8	*Strong*	21	13.58 ± 0.87	305.30 ± 6.32	15.35 ± 2.57
9	*Strong*	3	13.11 ± 0.63	319.97 ± 3.50	16.51 ± 3.43

5.2 Computation of the Wind Spectrum

The wind speed data is sampled at 1 Hz, hence a 10 minute data block should thus have 600 samples. Nevertheless, some blocks are, for several reasons, under-sampled. The analysis presented here uses only data blocks containing more than 540 samples. The algorithm used to compute the wind speed spectra is not affected by small gaps in the data series.

A normalized spectrum density for the horizontal wind speed μ was calculated for each 10 minutes block using the Lomb normalized periodogram (Press et al. 1994), which is used for spectral analysis of unevenly sampled data. The normalized periodogram was multiplied by $2\sigma^2$ (where σ^2 is the variance of the wind speed of each block) and divided by the sampling rate in order to get an individual spectrum density $S_\mu(n)$ in units of [(m/s)^2/Hz]. A dynamic response correction of each spectrum was performed using the empirical transfer function of the RISØ cup-anemometer (Yahaya and Frangi 2003; Kristensen and Hansen 2002).

In general, the wind spectrum density is usually analyzed against the normalized frequency $f = nz/U(z)$, known as the Monin (or similarity) coordinate, which is essentially the ratio of height to wavelength. The wind spectrum density is usually normalized in order to obtain the reduced spectrum $nS(n)/u_*^2$ of wind speed fluctuations, where the product $nS(n)$ (known as the non-normalized spectrum) of frequency n in Hz and the spectrum $S(n)$ is used so that the area between two frequencies represents the variance contributed by that frequency interval. $U(z)$ is the mean wind speed at height z, and the so called friction velocity u_* is a scaled velocity that represents the shear strength at the boundary layer and is calculated as (Simiu & Scalan, 1996)

$$u_* = \frac{kU(z)}{\ln(z/z_0)} \text{ [m/s]}, \tag{2}$$

where k is the Von Karman's constant (k = 0.4), and z_0 is the roughness length. The mean wind speed value in our database is approximately 8 m/s at z = 7.8 m height. We adopted a value of 0.03 m for z_0, using the tabulated values of Barthelmie et al. (1993) for ground without snow.

The reduced spectrum has been studied previously by Davenport and Kaimal (Davenport 1961, Kaimal et al. 1972 and 1976) who found an expression for the longitudinal wind speed fluctuations u, without significant influence from local features. The influence of local topography was analyzed by Antoniou and Antebi (Antoniou et al. 1992, Antebi et al. 1997) showing significant differences between the spectra computed for different wind directions.

5.3 Diurnal Wind Spectra

The nine general diurnal average spectra were computed by averaging all the spectra for each one of sectors 5, 6 and 7 and for the three wind speed ranges. These general average spectra were smoothed out by a running average of 5 data points. At the wind speeds and turbulence intensities registered in diurnal period (Table 5.2), the cup-anemometer presents nonlinear effects starting at n = 0.1 Hz, so the frequency components higher than this value were discarded.

Figure 5.1 shows the non-normalized general average spectra for the three sectors under each wind speed condition. No difference can be observed between the spectra of the three sectors studied under any wind speed condition, with exception of the *Strong* wind condition at which sector 5 seems to have a higher magnitude at the lower frequency range and slightly lower f_{max} frequency at which the spectrum reaches its maximum magnitude. However, this difference in the lower frequency range can be attributed to deviations introduced by the fewer amounts of data blocks available for sector 5 under *Strong* wind condition (see Table 5.2).

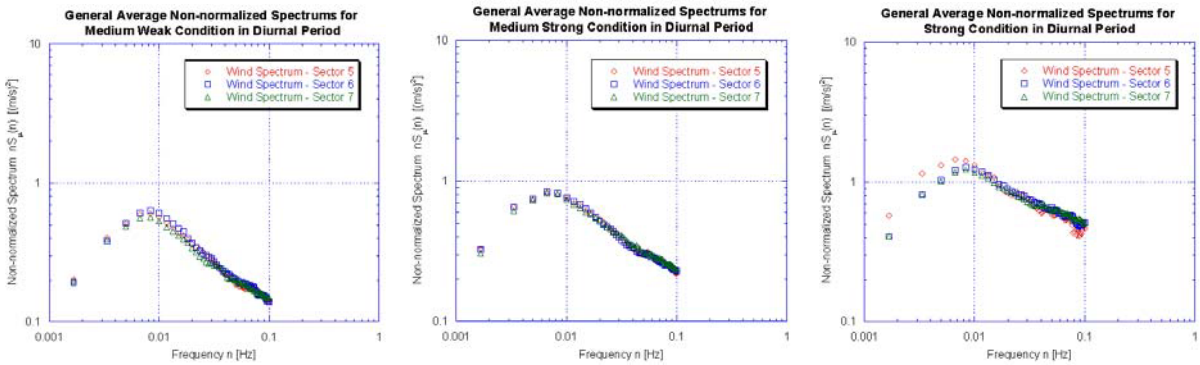

(a) (b) (c)

Figure 5.1 Non-normalized general spectra for (a) *Medium Weak*, (b) *Medium Strong* and (c) *Strong* wind conditions, in the diurnal period. These spectra showed no significant spectral difference between the sectors 5, 6 and 7.

5.4 Nocturnal Wind Spectra

For this case the topographic sectors analyzed were 7, 8 and 9. A general nocturnal average spectrum was computed for each sector, in the same way as we did for the diurnal case. At these magnitudes of wind speed and turbulence intensity (Table 5.3) the cup-anemometer presents nonlinear effects starting at n = 0.2 Hz, so for the nocturnal period the frequency components higher than this value were discarded.

Figure 5.2 shows the non-normalized general average spectra computed for the three sectors under each wind speed condition. In this case, the spectra have different shapes compared with the diurnal spectra. In the nocturnal spectra, two zones can be distinguished, the lower frequency range (frequencies lower than 0.01 Hz) and the higher frequency range (frequencies higher than 0.01 Hz). The difference within the nocturnal spectra is more evident under *Medium Weak* and *Medium Strong* wind conditions. The shape of the spectrum for these two wind conditions is the result of the combined effect of the transversal and longitudinal wind fluctuations (see equation 1), for stable atmosphere condition (Lumley and Panofsky 1964).

A number of 10 average spectra were obtained for each sector and wind condition. The 10 average spectra were formed from N/10 individual spectra, where N is the number of available data blocks in each sector (Table 5.3). Each average spectrum was smoothed out by a running average of 5 data points and then processed to get the reduced spectrum (see section 5.2). From each one of the 10 reduced average spectra, three features were extracted for the low and high frequency range: the maximum value S_{max}, the frequency $f_{\max}$, and the slope γ of the inertial subrange. The latter was obtained by fitting the model in equation (3) to the reduced average spectra.

$$\frac{nS_{\mu}(n)}{u_{*}^{2}} \approx \alpha f^{-\gamma} \tag{3}$$

A Kruskal-Wallis (KW) statistical comparison test was applied to each feature extracted from the 10 average reduced spectra found for each of the three sectors and to validate the statistical differences we have previously noticed. This nonparametric test compares populations with unknown distributions and tests the null hypothesis, with 95% of confidence, that p samples from possibly different populations actually originate from similar populations, at least as far as their central tendencies, or medians, are concerned (Hollander and Wolfe 1973, Hochberg and Tamhane 1987).

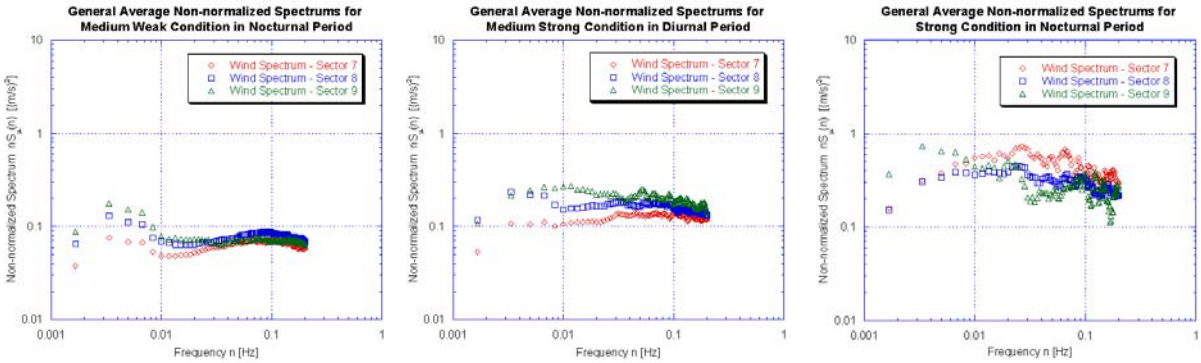

(a) (b) (c)

Figure 5.2 General average wind spectra for (a) *Medium Weak*, (b) *Medium Strong* and (c) *Strong* wind conditions, in the nocturnal period. The spectrum of sector 7 showed significant difference with respect to the spectra of sector 8 and 9, for the *Medium Strong* wind condition.

For *Medium Weak* wind speed condition, the KW test showed no significant difference between the three topographic sectors. For *Medium Strong* wind condition this statistical test showed significant differences only between the S_{max} values of the low frequency range for sector 7 when compared with sectors 8 and 9. The available data for the *Strong* wind condition was considered too few to perform this statistical test (see Table 5.3).

6. Discussion of the Results

The wind spectra found in Chapter 5 shows a clear difference between the diurnal and nocturnal periods. During the diurnal period the intensity of the wind spectra is higher than during the nocturnal time, thus indicating a lower energy level in the wind turbulence.

In order to explain the difference between the diurnal and nocturnal wind spectra, we have to go back to the way the instrument works, as we explained in section 3.1. The cup-anemometer measures both the transversal *v* and longitudinal *u* fluctuations of the wind, as shown in equation (1). Thus, the intensity and shape of the spectra for each of these two wind components are produced by thermal instability in the boundary layer (Lumley and Panofsky 1964). Increased thermal instability greatly increases the intensity of the low frequency portion of the spectrum, but leaves the high-frequency portion relatively unaffected. Consequently, at any given wind speed, the effect of an increasing temperature lapse rate is to superimpose long-period variations on top of the shorter mechanically produced variations. For the transversal wind component, the low frequency region of the spectrum is mostly dependent on the temperature lapse rate, whereas the high-frequency region is affected by both the ground roughness and wind speed. On the other hand, mechanical turbulence (wind shear and surface roughness) on the longitudinal wind component has a stronger influence on the high-frequency region and, to some extent less importantly, in the low frequency part of the spectrum (Lumley and Panofsky 1964).

The influence of thermal stability on the shape and intensity of the wind spectra can be noticed by comparing the spectra in Figures 5.1 and 5.2. Near the ground, during periods of clear sky, the boundary layer generally presents stable conditions during night time and unstable conditions during daytime. During the diurnal period, the intensity in the low frequency regions of the wind spectra is severely affected by the unstable atmosphere (i.e. the convective turbulence), whereas the mechanical turbulence affects its high frequency part. The effect of wind shear and ground roughness increases the intensity of the spectra and the slope of the inertial subrange decreases as the mean wind speed increases, as we can clearly see in the plot sequence in Figure 5.1. During the nocturnal period the atmosphere is stable, which makes the effect of mechanical turbulence to dominate the shape and intensity of the wind spectra. This is the reason explaining the differences between the wind spectra

from sector 7 when compares against sector 8 and 9 for the night time condition, as seen in Figure 5.2b. This difference can be attributed to the local topography. Figure 6.1 shows the upwind surface profile for Chajnantor area, starting from the wind anemometer mast position. The surface profile of sector 7 is clearly different from sectors 8 and 9, which are quite similar up to about 1100 m from the wind sensor mast. The surface profile of sector 9 is significantly different from sectors 7 and 8 beyond 1100 m from the mast, which also includes the north-east side of *Cerro Chico* (a peak about 100m higher than the surrounding plateau). Therefore, the fact there are no significant differences in the shape and magnitude of the *Medium Weak* wind spectra (Figure 5.2a) for sector 8 and 9, suggests the relevant topographic influence seems to come from the first 1 km of distance from the mast for this range of wind speed. In the case of the *Medium Strong* wind condition (Figure 5.2b) we see the wind spectra for sectors 8 and 9 to have a slight difference in the middle frequency part (frequencies between 0.009 and 0.03). This difference may have origin in the difference in the topography profile beyond 1 km upwind from the mast. However, for the case of the *Medium Strong* and *Strong* wind conditions we do not count with enough data during night time for these three sectors. Consequently, we can not conclude with certainty whether the topography at long distances is of relevance for the wind spectra or not at these wind ranges.

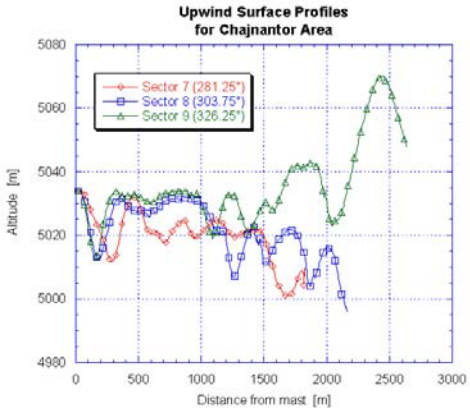

Figure 6.1 Upwind surface profiles of Chajnantor area for sectors 7, 8 and 9 from the cup-anemometer mast. In the sector 9 there are larger undulations than in sector 7. Also these undulations increase their altitudes as distance from mast increased, contrary to sector 7 where the altitude of the undulations decrease with the distance from mast. Sectors 8 and 9 are quite similar up to about 1100 m from mast.

7. Comparison with the Wind Model used for the Design of the ALMA Antennas

In order to estimate the effect of wind loads over the structures of the ALMA antennas, a wind spectrum density model, proposed by Kaimal (1972) for structural design purposes, was used for the antenna specifications. The model used for ALMA is described by the following equation:

$$S(n) = \frac{u_*^2}{n} \frac{af}{(1+bf)^{5/3}}, \tag{4}$$

where a = 200, b = 50 (Simiu and Scalan 1996), f is the normalized frequency and u_* is the friction velocity computed from (2) with z = 7.5m, z_0 = 0.05m and considering a mean wind speed $U(z)$ of 6m/s for day time condition and 9m/s for night time, values adopted in the design specifications for the primary operation conditions. For design purposes the antenna specifications have been set such as for day time conditions the main deformations to deal with are thermal deformations and a wind load for winds up to 6 m/s. On the other hand, for night time conditions the thermal deformations are very small due to the fact the temperature gradients are negligible, so a wind load for winds up to 9 m/s has been adopted.

Figures 7.1a and 7.1b show the result for the average wind spectrum densities, which have been computed by weighting all spectra recorded at each topographic sector and for all the wind speed conditions considered in this analysis (see Chapter 5). Both plots also include the Kaimal's model used in the antenna specifications for the diurnal and nocturnal periods.

Figure 7.1a shows that the model used for the antenna design fits bellow the wind spectra for *Medium Strong* condition. However, we understood that designing an antenna to deal with full thermal deformation, and also for all conditions of wind load, it was a technological challenge associated to a very high price. The wind spectrum used in the specifications for day time conditions shows the best compromise between the real conditions of the site, regarding temperature and wind load, and the total cost of the technical solution for the antenna design. On the other hand, as have we see in Figure 7.1b, the model for the wind spectra for night time condition is placing an upper limit to the wind conditions at the site. This, together with the negligibly thermal deformations, will provide us with an antenna expected to show a great mechanical performance during night time observations.

Due to the sampling rate and the non-linear effects, we are only able to observe frequency components of the spectra up to 0.2 Hz. Because the natural frequencies of the ALMA antenna structure are higher than 0.03 Hz, the low frequency part of the spectra is of less importance for the ALMA antenna design. In order to estimate the spectral behaviour at higher frequencies, a model for each wind condition and daily cycle has been fitted to the measured spectra.

The high frequency part ($n \geq 0.01$Hz) of the diurnal spectra was modelled using equation (3). The high frequency parts ($n > 0.03$Hz) of the nocturnal spectra were modelled using equation (4) with the exception of the spectrum for *Strong* wind condition which can be fit over the whole frequency range. In these models, the friction velocity u_* and the normalized frequency f were computed using the parameters described in Chapter 5 and with $U(z)$ corresponding to an upper limit wind speed for each wind interval condition. The fitted models are shown in Figure 7.2 together with the spectra, and their respective parameters are summarised in Table 7.1. The parameters of these models were computed for the reduced mean spectra. These models were fitted as an envelope of the spectra.

In order to find a relation between the spectral behaviour of the wind and the mean wind speed at Chajnantor, we show in Figure 7.3 the parameters of the models (Table 7.1) versus the extreme mean wind speed of each wind condition. In this figure it can be seen that the parameters of the models, for diurnal and nocturnal periods, present approximately an exponential relation with the mean wind speed. These exponential relations are summarized in Table 7.2.

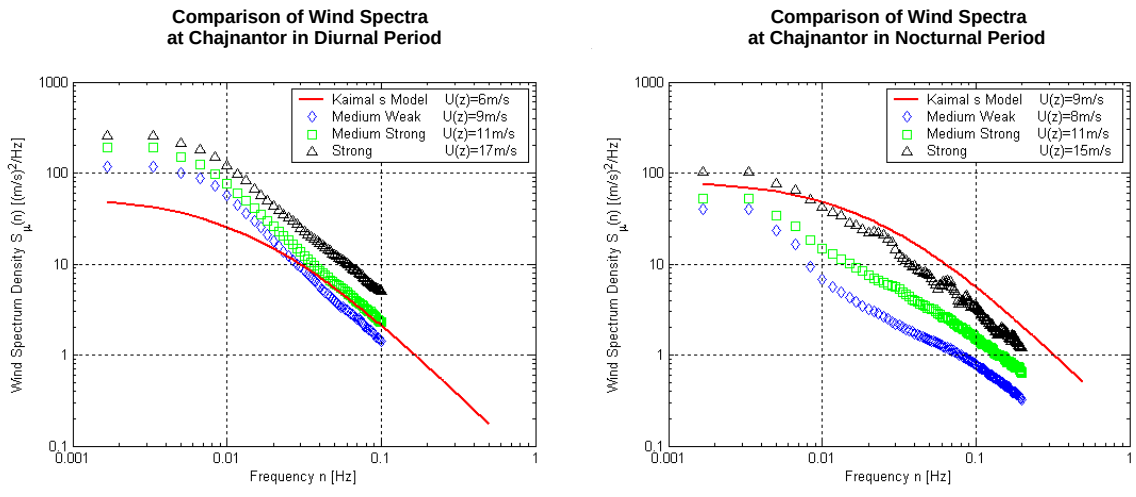

(a) (b)

Figure 7.1 Comparison between the spectrum density obtained for the three wind speed conditions and the model used in the ALMA antenna specifications, for (a) diurnal and (b) nocturnal periods. The spectra estimated are the weighted (with the number of available data blocks) average of the general average spectra from sectors 5, 6 and 7 in diurnal period, and for sectors 7, 8 and 9 in nocturnal period

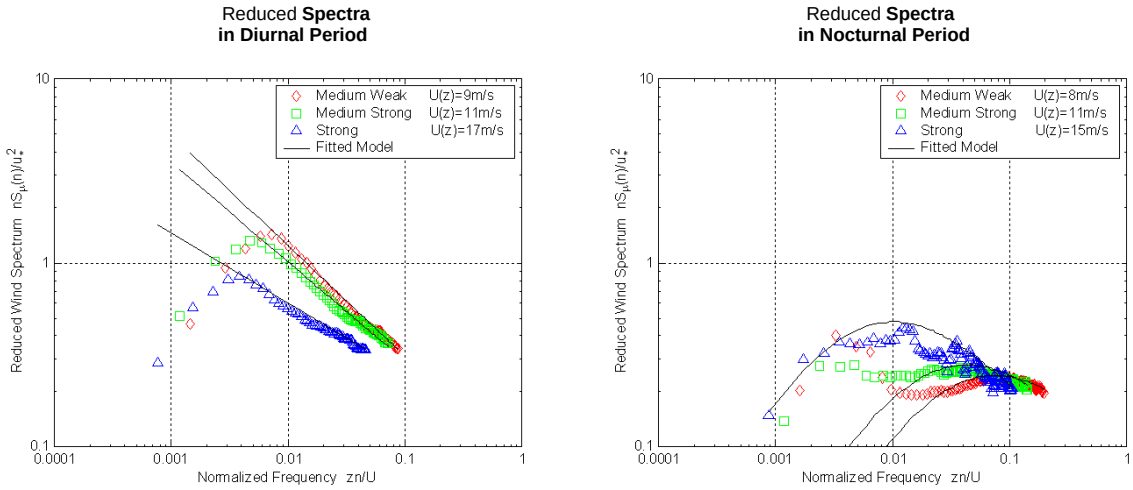

(a) (b)

Figure 7.2 Reduced spectra and their respective fitted models for (a) Diurnal period and (b) Nocturnal period.

TABLE 7.1, MODELS OF THE REDUCED SPECTRA FOR EACH WIND SPEED CONDITION, FOR THE DIURNAL AND NOCTURNAL PERIODS.

	Diurnal Period		***Nocturnal Period***	
Wind Condition	*U(z)* [m/s]	Model (n>0.01Hz)	*U(z)* [m/s]	Model (n>0.03Hz)
Medium Weak	9	$0.063 f^{-0.65}$ f>0.0087	8	$\frac{15 f}{(1+20 f)^{5/3}}$ f>0.03
Medium Strong	11	$0.094 f^{-0.52}$ f>0.0071	11	$\frac{30 f}{(1+35 f)^{5/3}}$ f>0.02
Strong	17	$0.105 f^{-0.38}$ f>0.0046	15	$\frac{220 f}{(1+150 f)^{5/3}}$ f>0

The relations in Table 7.2 are useful to estimate the high frequency part of the spectra for different mean wind speeds at Chajnantor. In Figure 7.4 it can be seen that the model specified for primary operation conditions of the ALMA antennas is limited by a mean wind speed of about 10m/s during the diurnal period. During the nocturnal period, the Kaimal's model becomes the top level of the nocturnal wind spectra at frequencies higher than 0.1Hz. These models only give an estimation of the average horizontal wind spectrum, so the antennas operation actually will be determined by the thermal deformations, the spectral response of the antenna structure and the effective wind loads produced by the longitudinal, transversal and vertical components of the wind fluctuations at Chajnantor.

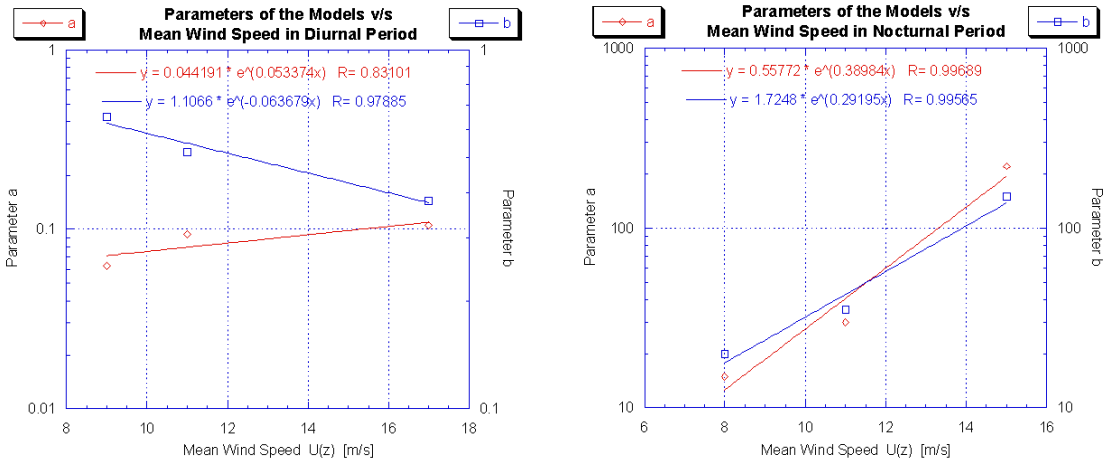

(a) (b)

Figure 7.3 Relation between the parameters of the models fitted and the extreme mean wind speed of each wind condition in (a) diurnal period and (b) nocturnal period.

TABLE 7.2, EXPONENTIAL RELATIONS FOR THE PARAMETERS OF THE MODELS AND THE MEAN WIND SPEED AT CHAJNANTOR, FOR THE DIURNAL AND NOCTURNAL PERIODS.

	Diurnal Period (a,b)	***Nocturnal Period (α γ),***
Parameter	Function of *U(z)*	Function of *U(z)*
a / α	$0.044e^{0.053U(z)}$	$0.558e^{0.390U(z)}$
b / γ	$1.107e^{-0.064U(z)}$	$1.725e^{0.292U(z)}$

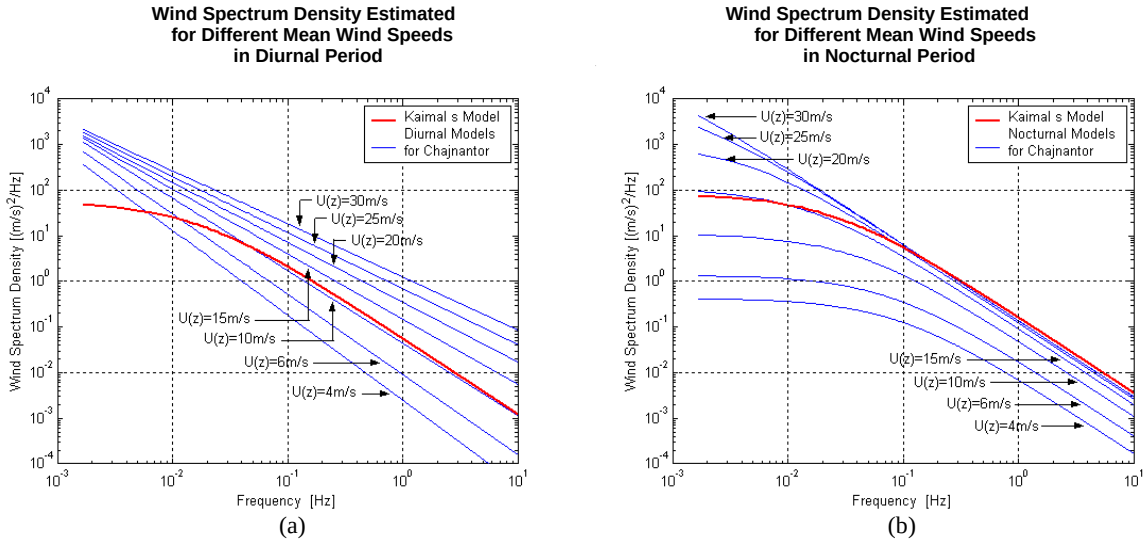

(a) (b)

Figure 7.4 Wind spectrum densities estimated for different mean wind speed in (a) Diurnal period and (b) Nocturnal period, compared with the Kaimal's model used in the specifications for the ALMA antennas. The spectra are estimated for a mean wind speed *U(z)* of 4m/s, 6m/s, 10m/s, 15m/s, 20m/s, 25m/s and 30m/s, from bottom to top, respectively.

8. Conclusions

Considering the available wind data for 2001 and 2002, Four wind speed conditions (*Weak, Medium Weak, Medium Strong* and *Strong*) were defined based on a statistical criteria as explained in section 4.1. Two markedly different daily periods (*diurnal* and *nocturnal*) were defined based on a threshold value for the wind speed described in section 4.2. We further classified the wind speed at Chajnantor based on wind speed direction, and with the aim to study the effect of the topography features in the spectral structure of the wind.

Concerning the classification of the wind in four wind conditions we can confirm that the energy of the spectra is proportional to the mean wind speed.

Regarding to the *diurnal* and *nocturnal* classification of the wind we conclude that, for a given wind speed condition, the energy content of the wind spectra is higher during day time compared with the night time. Specifically, we see differences in the frequency at the peak amplitude of the spectra and the slope of the inertial subrange as can be seen in sections 5.3 and 5.4. The low frequency part of the diurnal spectra shows a clear influence of the convective turbulence, meanwhile the nocturnal spectra are mainly dominated by the shear stress and surface roughness.

With respect to the wind direction, during daytime, we have not seen a mayor effect of the topography in the spectral structure of the wind, which is mainly dominated by the convective turbulence in the boundary layer, as stated in the previous paragraph. The exception is the case of the night time *Medium Strong* wind condition where we noticed a difference in the structure of the wind spectra for a particular topographic sector. A particular parameter of the wind spectra for this particular sector (sector 7) was found to be statistically different respect to the corresponding parameter of the other sectors with 95% confidence. The difference we have found consists basically in the fact the wind spectra of this sector shows a low energy content for frequencies bellow than 0.1 Hz.

Spectral models were fitted to the high frequency part of the wind spectra obtained at Chajnantor for the diurnal and nocturnal periods, for the *Medium Weak, Medium Strong* and *Strong* wind speed conditions. Exponential relations were found between the parameters of these models and the wind speed conditions at Chajnantor, which makes possible to estimate the spectral behaviour of the wind for different mean wind speeds.

Finally our comparison of the wind spectra we have obtained for winds in the range of the 6 m/s and 9 m/s at Chajnantor both shows low energy content when compared to the model used for the design of the ALMA antenna. We can infer this directly from Figure 7.1 and from Figure 7.4. This in fact imply that mechanical performance of the ALMA antennas, regarding wind load, is expected to be even better for both the day time and night time conditions.

9. Further Suggested Work

9.*1 Seasonal Analysis of the Wind Turbulence*

The wind speed data base can be analyzed to look for seasonal effects. A study like this might be of relevance for the planning of ALMA operations including the configuration of the array and scheduling of a particular frequency band for observation.

9.2 Computing 3D Components of the Length Scale

The theory explains that there are nine integral length scales of wind turbulence. These correspond to a measure of the average size of the three dimensional eddies of the wind flow (Simiu and Scalan 1996). These can be obtained from the wind speed fluctuations in the longitudinal, transversal and vertical components of the wind, *u*, *v* and *w*.

With the help of an anemometer capable to measure the three components of the wind speed, the integral length scales of the turbulence can be determined. The analysis of the turbulence length scales is very important for the estimation of the wind loading on the antenna structure and to estimate whether the effective turbulence at Chajnantor would be significant or not (Simiu and Scalan 1996).

9.3 Estimation of the Local Roughness Lengths

The roughness length z_0 used in this work was assumed as 0.03 m for the ground conditions at Chajnantor, according to tabulated z_0 values found at (Barthelmie et al. 1993). For completeness we can mention that for the ground cover by snow a more appropriate value of z_0 is 0.005 m.

A more accurate estimation of the local roughness length z_0 can be accomplished by using wind speed data gathered at two significantly different heights from the ground. A possible method for the determination of z_0 has been suggested by (Barthelmie et al. 1993) and we included it here for completeness.

The method suggested by Barthelmie is based on a logarithmic profile for the wind (Equation 2) under neutral atmospheric conditions, which can be regarded as applying approximately when wind speeds are greater than 6 m/s (Wieringa 1976). Thus, if we know the wind speed U_1, at a height z_1, and at the same time the wind speed U_2, at a height z_2, the following expression can be deduced from (2):

$$\frac{U_1}{U_2} = \frac{\ln(z_1/z_0)}{\ln(z_2/z_0)}, \tag{9}$$

hence, the roughness length can be computed as in equation (10).

$$\ln(z_0) = \frac{U_1 \ln(z_2) - U_2 \ln(z_1)}{U_1 - U_2}. \tag{10}$$

In order to have reliable estimates of z_0, reasonable confidence in the quality of the wind speed measurements is required since errors in one of the measured values will give large errors in the roughness length due to the anti-log part of the equation.

Acknowledgments

We are a lot grateful to Doctor Joseph Antebi from Simpson Gumpertz & Heger Inc, who kindly provided relevant information and documentation about previous works carried out for Large Millimeter Telescope project. The wind database and the whole atmospheric instruments installed at Chajnantor are maintained in operation by Roberto Rivera and Simon Radford.

References

Antebi J., Zarghamee M. S., and Kan F. W., 1997. “Wind Characterization and Beam Pointing Error - Large Millimeter Telescope”. SGH Report to LMT Project Office.

Antoniou I., Asimakopoulos D., Frangoulis A., Kotronaros A., Lalas D.P. and Panourgias I., 1992. “Turbulence measurements on Top of a Steep Hill”. Journal of Wind Engineering and Industrial Aerodynamics. 39, pp 343 – 355.

Barthelmie R.J., Palutikof J.P. and Davies T.D., 1993. “Estimation of Sector Roughness Lengths and The Effect on Prediction of the Vertical Wind Speed Profile”. Boundary-Layer Meteorology. 66, pp 19 – 47.

Bustos R., Delgado G., Nyman L., and Radford S., 2000. “52 Years of Climatological Data for the Chajnantor Area”. ALMA memo No. 333.

Davenport G., 1961. “The Spectrum of Horizontal Gustiness Near the ground in High Winds”. Quart. J. Royal Meteorology Soc., 87, 194.

Hiriart D., Ochoa J. L., and García B., 2001. “Wind Power Spectrum Measured at The san Pedro Mártir Sierra”. Astronomy and Astrophysics Mexican Magazine. No. 37, pp 213 – 220.

Hochberg Y., and Tamhane A.C., 1987. “Multiple Comparison Procedures”. Wiley.

Hollander M., and Wolfe D.A., 1973. “Nonparametric Statistical Methods”. Wiley.

Kaimal J.C.,Wyngaard J.C., Izumi Y. and Coté O.R., 1972. “Spectral Characteristics of Surface-Layer Turbulence”. Quart. J. Royal Meteorology Soc., 98, pp 563 – 589.

Kaimal J.C.,Wyngaard J.C., Haugen D.A., Coté O.R. and Izumi Y., 1976. “Turbulence Structure in the Convective Boundary Layer”. Journal of the Atmospheric Sciences, 33, pp 2152 – 2169.

Kristensen L. and Hansen O.F., 2002. “Distance Constant of the RISØ Cup Anemometer”. Risø National Laboratory, Roskilde, Denmark.

Lumley J. L. and Panofsky H. A., 1964. “The Structure of Atmospheric Turbulence”, Wiley & Sons.

Pedersen T.F., 2003. “Characterization and Classification of RISØ P2546 Cup Anemometer”. Risø National Laboratory, Roskilde, Denmark.

Press W. H., Teukolsky S.A., Vetterling W.T. and Flannery B.P., 1994. “Numerical Recipes in C, The Art of Scientific Computing”. Cambridge, 2nd Edition.

Radford S. J., 2004. “Chajnantor Windroses”. ALMA memo 485.

Simiu, E., and Scalan, R. H., 1996. “Wind Effects on Structures: Fundamentals and Applications to Design”. 3rd Ed. (New York: Wiley).

Smith D., Paglioni T.A., Lovell A.J., Ukita N., and Matsuo H., 2000. “Measurements of Dynamic Pointing Variations of a Large Radio Telescope”. Proc. SPIE, Vol. 4015, p. 467.

Wieringa J., 1976. “An Objective Exposure Correction Method for Average Wind Speeds Measured at a Sheltered Location”. Quart. J. Royal Meteorology Soc., 102, pp 241 – 253.

Yahaya S. and Frangi J.P., 2003. “Spectral Response of Cup Anemometers”. Laboratorie Environnement et Développement, CP 7071, Université Paris 7, France.

Appendix

Comparison of the Wind Data Registered by the Different Anemometers Installed at Chajnantor Site

Tables 1, 2 and 3 show the statistics computed from wind speed data registered at Chajnantor by the cup-anemometer (ESO), the propeller-anemometer (NRAO), weather station B (which is located near the site testing containers) and the Davis station (located on the container ESO1).

Table 1 summarizes the statistics for the period February 12th through 28th 2002. The differences observed in the statistical median values are negligible between the propeller and the cup anemometers, but are within 1 m/s with respect to the Davis.

Table 2 shows a discrepancy in the statistics calculated from wind speed data gathered with the four instruments is of the order of 1 m/s. Here the difference in the statistics might be attributed to the fact the four instruments present different amount of data gathered in the period under analysis (October 1st through 31st).

Table 3 shows the statistics computed from the wind data gathered during the month of November 2001. The ESO's cup anemometer and weather station have comparable amounts of data. The NRAO propeller anemometer's data has about 20% less time coverage this month. Despite of the difference in the amount of data the statistics are comparable and within ±0.5 m/s.

TABLE 1 WIND SPEED STATISTICS FOR DAYS 12 THROUGH 28, FEBRUARY 2002.

Instrument	Available Data [%]	Median Wind Speed [m/s]	Mean Wind Speed [m/s]	Max Wind Speed [m/s]	Min Wind Speed [m/s]
Cup-Anemometer	52.34	4.93	5.57	18.29	0.57
Propeller Anemometer	40.12	4.59	5.03	16.59	0.023
Weather Station B	57.59	4.20	4.73	11.90	0.10
Davis Station	100.00	4.00	4.61	12.10	0.0

TABLE 2 WIND SPEED STATISTICS FOR DAYS 1 THROUGH 31, OCTOBER 2001.

Instrument	Available Data [%]	Median Wind Speed [m/s]	Mean Wind Speed [m/s]	Max Wind Speed [m/s]	Min Wind Speed [m/s]
Cup-Anemometer	91.14	7.42	7.77	27.93	0.57
Propeller Anemometer	72.31	6.58	7.05	25.70	0.0
Weather Station B	50.40	7.60	8.18	19.50	0.0
Davis Station	99.98	6.70	6.73	22.40	0.0

TABLE 3 WIND SPEED STATISTICS FOR DAYS 1 THROUGH 30, NOVEMBER 2001.

Instrument	Available Data [%]	Median Wind Speed [m/s]	Mean Wind Speed [m/s]	Max Wind Speed [m/s]	Min Wind Speed [m/s]
Cup-Anemometer	92.82	6.31	6.93	27.31	0.57
Propeller Anemometer	71.62	5.81	6.47	26.15	0.023
Weather Station B	94.76	5.20	5.82	16.30	0.0
Davis Station	100.00	5.40	5.88	17.90	0.0

Figure 1(a) shows wind speed data gathered with the four different instruments over two days. The days covered by this plot are November 1 and 2, 2001. The data has been plotted using their particular sampling rates (one sample each 1 second for the cup-anemometer; one sample each 10 minutes for the propeller-anemometer; an hourly average for the weather station B; and a 5 minutes average for the Davis station). No averages have been done on the original series; we expect the trends to be the same but the noise is lower in the case of the ESO's weather station B due to the one hour average samples provided by this instrument.

From Figure 1(b) we see a good agreement between the ESO's cup anemometer and the NRAO's propeller anemometer. Some differences are evident at low values of wind speed. The difference might be attributed to the combined behavior and performance of mechanical devices (vertical axis rotating cups, and horizontal axis rotating propellers) with low wind flows. In this brief look the ESO's weather station and the Davis station data appears to have a negative offset when compare with the trend of the other two instruments. This can be seen in the lower values for the wind speed statistics computed out of these data set as seen in Table 4. Still all the statistics are within 1 m/s of wind speed.

The negative offset of the weather station B could be due to a calibration problem of the weather station instruments (since the last calibration was made at the end of 1999). Also the offset of the Davis and the weather station B could be due to their anemometers are located at a height lower than the cup and propeller anemometers. On the other hand, the cup-anemometer will never register a value of zero because it is calibrated from factory with an offset of 0.255 m/s at zero wind speed.

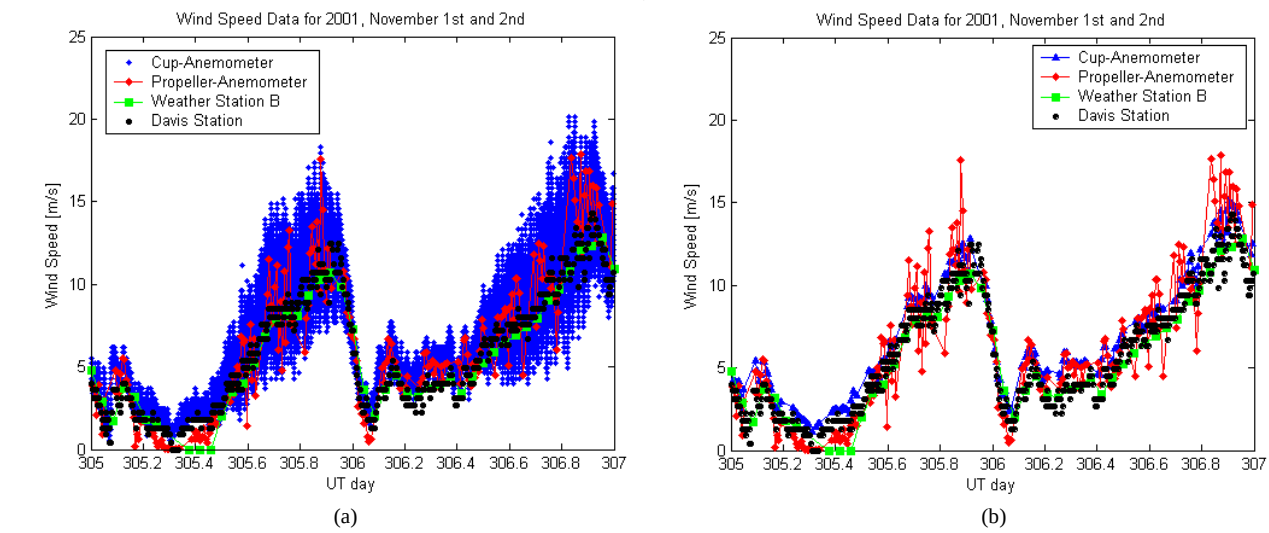

Figure 1 Wind speed data registered by the cup-anemometer, the propeller-anemometer and the weather station B (in front of the NRAO container) for the period November 1st and 2nd of the year 2001. (a) Shows the total samples registered at 1 Hz by the cup-anemometer. (b) Shows the average each 10 minutes of the cup-anemometer series. The noise level of the propeller is due to this instrument does not take an average, just one sample each 10 minutes.

TABLE 4 WIND SPEED STATISTICS FOR DAYS NOVEMBER 1st AND 2nd OF THE YEAR 2001.

Instrument	Available Data [%]	Median Wind Speed [m/s]	Mean Wind Speed [m/s]	Max Wind Speed [m/s]	Min Wind Speed [m/s]
Cup-Anemometer	92.73	5.85	6.80	20.16	0.57
Propeller Anemometer	72.22	5.34	6.36	17.86	0.023
Weather Station B	97.92	4.80	5.74	12.80	0.0
Davis Station	100.00	4.70	5.76	14.30	0.0